NATURAL SCIENCE REVIEW 3 200602 (2026)
nsr.jinr.int

# Study of low-energy QCD in meson reactions with the Coulomb field of atomic nuclei

A. Guskov*[1], A. Maltsev†[1,2], and A. Olshevskiy‡[1]

[1] *Joint Institute for Nuclear Research, Dubna, Russia*
[2] *Technical University of Munich, Munich, Germany*

**Abstract**

This paper reviews the development of theoretical and experimental studies of low-energy QCD parameters starting from early investigations at the JINR Laboratory of Theoretical Physics and ending with modern measurements at CERN. We summarize the historical background and the pioneering theoretical approaches used at JINR to calculate meson parameters in various hadronic models which have laid the foundation for the experimental proposal to investigate the pion polarizability via radiative scattering off nuclei. The first observation of the Compton effect on the pion and the first measurements of the charged pion polarizability and the $\gamma \to 3\pi$ constant performed with the U-70 accelerator are discussed as key milestones enabling quantitative studies of the meson structure and highlighting their impact on the low-energy QCD phenomenology. Continued advances in theoretical predictions have underscored the need for higher-precision experimental data and motivated new measurements carried out with pion beams in the COMPASS experiment at CERN. Finally, we outline the prospects for future studies within the AMBER experiment where kaon beams will enable a precision determination of kaon polarizabilities and related low-energy constants further advancing our understanding of dynamics of the strong interaction.

*Keywords:* low-energy QCD, meson polarizability, chiral anomaly

DOI: 10.54546/NaturalSciRev.200602

## 1. Introduction

It is well known that the theory describing strong interactions between elementary particles is Quantum Chromodynamics (QCD), based on the concept of color quarks and gluons as constituent parts of hadrons and carriers of strong interactions. However, a peculiarity of these objects is that they cannot be observed in a free state, which makes QCD significantly different from, for example, Quantum Electrodynamics (QED).

In fact, this leads to the existence of two limiting regimes: small distances ($\ll 1$ fm) — where quarks become asymptotically free and the perturbation theory is applicable; and large

*Corresponding author e-mail address: avg@jinr.ru
†Author e-mail address: andrii.maltsev@cern.ch
‡Author e-mail address: olshevsk@jinr.ru

Received: 8 December 2025; Revised: 2 February 2026; Accepted: 2 February 2026; Published: 27 February 2026

distances ($\gtrsim 1$ fm) — where quarks experience confinement and calculations must be performed in the nonperturbative regime. Despite the complexity of calculations in this area, the information extracted from comparisons with fexperimental data is of considerable interest for testing the theory. And since the middle of the last century, many models and approaches for performing such calculations have been developed, including low-energy theorems and QCD sum rules, lattice calculations, descriptions using the Chiral Perturbation Theory (ChPT), and others.

The ChPT has gained a particular popularity as an effective low-energy theory of QCD, historically linked to earlier approaches of partial conservation of axial current (PCAC). It allows calculations of low-energy parameters describing the interactions of mesons and nucleons at low energies. The small parameter used in this decomposition is the momentum of interacting particles compared to the typical scale of hadron masses of about 1 GeV ($\rho$-meson, proton). And the "observables" for the comparison with the experiment are, for example, the lengths of pion–pion scattering which describe this simplest but fundamentally important for ChPT example of the interaction of two hadrons.

Other important parameters characterizing the hadron $h$ are its electric $\alpha_h$ and magnetic $\beta_h$ polarizabilities. Along with the mass, radius, and magnetic moment, they are fundamental constants describing the response of the hadronic structure to the external electromagnetic field.

The polarizabilities are introduced as coefficients of the low-energy expansion of the Compton scattering amplitude, i.e., the electromagnetic interaction of the particle with photons. However, their values clearly characterize the "rigidity" of the hadron as a complex QCD system. In the nonrelativistic approximation, dipole polarizabilities can be treated as coefficients of the proportionality between the strength of the external electric ($\vec{E}$) and magnetic ($\vec{H}$) field and the corresponding induced dipole moment:

$$\vec{P} = \alpha_h \vec{E}, \tag{1}$$

$$\vec{\mu} = \beta_h \vec{H}. \tag{2}$$

Thus, the measurement of hadron polarizabilities in comparison with theoretical expectations tests the low-energy QCD and various phenomenological models.

By the end of the 1970s, polarizabilities for some hadrons have been already calculated using different approaches and models, in particular, by scientists from the JINR Laboratory of Theoretical Physics. For the charged pion, for example, this was done in [1–5]. In addition, a number of reviews appeared discussing the proton polarizability measured at that time and pointing to the importance of performing measurements for other particles.

From the theoretical point of view, the most interesting quantity is the polarizability of the lightest quark system — the pion. However, from the experimental point of view, the possibility of organizing scattering of a pion off a photon is low due to the absence of both pion and photon targets.

Nevertheless, an interesting possibility for such measurements was presented in [6]. It was proposed to measure the polarizability of the charged pion by studying its scattering off the virtual photon of the Coulomb field of the nucleus, and, in the final state, to detect the scattered pion and the scattered photon which turned in this reaction from the virtual to the real one. In a sense, this extends the idea of using the Coulomb field of the nucleus as a source of (virtual) photons which was originally proposed by Henry Primakoff for measuring the lifetime of the neutral pion.

It was shown in [6] that in the reaction of pion–nucleus scattering with a photon emission (radiative scattering) at low momentum transfers to a nucleus squared ($Q^2 < 2\times10^{-4}$ GeV$^2/c^2$), the contribution of electromagnetic scattering will dominate over that of strong scattering.

By selecting such events, we will be effectively dealing with the pion Compton scattering. It was also shown in [6] that such scattering with the hard photon in the final state will be sensitive to polarization effects allowing for the first measurement of the polarizabilities for the charged pion.

The proposed experiment was set up by a group from JINR and IHEP at the Serpukhov accelerator, and the results of the first observation of the Compton effect on the pion and the first measurement of the polarizabilities of the charged pion were published in [8] and [9], respectively.

The measured values of pion polarizabilities became an important stimulus for revising models and improving the accuracy of calculations of this quantity, as well as for implementing other experimental ideas for measuring polarizabilities in the scattering of photons off the virtual pion "coat" of the nucleus and the production of pion pairs in $\gamma\gamma$ interactions at $e^+e^-$ colliders. However, for a long time, the result obtained from radiative scattering remained the most accurate measurement and the reliable theoretical interpretation.

The results of the experiment gained with the Serpukhov accelerator are not merely the observation of the Compton effect and the measurement of polarizabilities. Another fundamentally important result was obtained in the study of the process of conversion of the pion incident on the nucleus Coulomb field (i.e., at low momentum transfers) into a pion pair. The cross section of this process depends on the diagram with the connection of one photon with three pions which is calculated in the theory with chiral anomalies. The result for the first-ever $\gamma \to 3\pi$ constant was found to be in agreement with the calculations performed within the framework of this theory.

## 2. Primakoff measurements with the SIGMA spectrometer

On the one hand, as already mentioned, to experimentally observe the pion Compton scattering is difficult due to the absence of pion and photon targets. On the other hand, the idea of exploiting the nuclear Coulomb field as a source of quasi-real photons was already proposed and successfully used by Henry Primakoff in measuring the neutral pion lifetime [7]. In the community, the extension of this idea to other processes acquired the name "Primakoff reactions".

In the early 1980s, following the original proposal in [6], the reaction of pion radiative scattering in the Coulomb field of nuclei (i.e., at low momentum transfers to nuclei)

$$\pi^- + (A, Z) \to \pi^- + (A, Z) + \gamma \tag{3}$$

was used to observe the pion Compton effect for the first time and to measure the pion polarizabilities.

In addition, the reaction of pion pair production by pions at low momentum transfers to nuclei

$$\pi^- + (A, Z) \to \pi^- + (A, Z) + \pi^0 \tag{4}$$

allowed the measurement of the $\gamma \to 3\pi$ chiral anomaly.

The experiment was carried out with the Serpukhov accelerator using the existing SIGMA spectrometer and the additional detector of photons constructed especially for this programme. The details of the experimental setup can be found in [10].

The main challenge of the constructed setup was to provide an accuracy of the measurement of the momentum transfer to nuclei which should allow selecting the Coulomb interaction of photons from nuclei. The layout of the experimental setup is presented in Fig. 1.

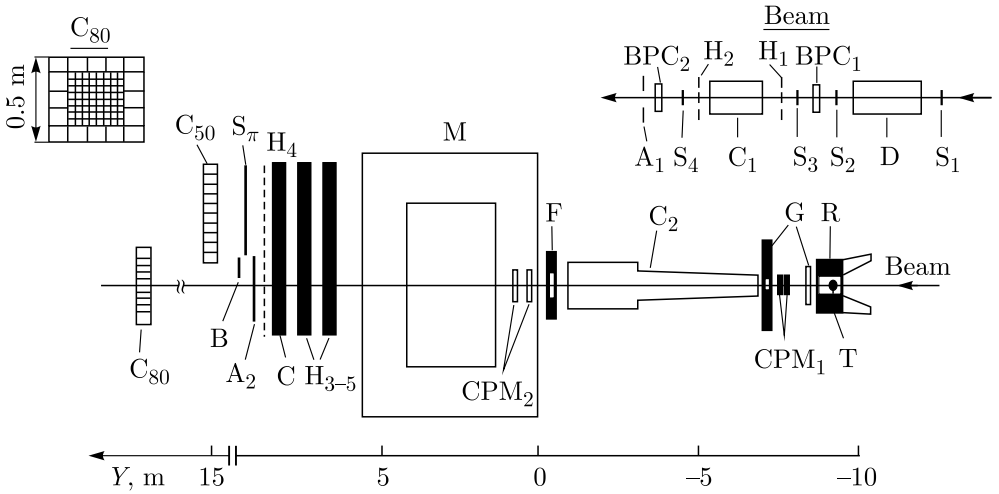


**Figure 1.** SIGMA spectrometer layout [12].

The 40 GeV/$c$ pion beam was identified and measured by the threshold and differential gas Cherenkov counters, scintillating hodoscopes, and proportional chambers. Beam particles were bombarding the target of the 0.25 radiation length ($X_0$) thickness, and the scattered pion was detected by the magnetic spectrometer with proportional and spark chambers and the scintillating hodoscope. The energy and position of the photon(s) were measured by the electromagnetic calorimeter made of lead glass counters. The trigger required the beam and scattered particle tracks, no signal in the veto around the target and in the forward Cherenkov detector with the threshold of 18 GeV/$c$ and the energy in the electromagnetic calorimeter above 5 GeV.

Such requirements allowed selecting event signatures where the primary pion looses a significant part of its energy (more than a half) while there are no wide angle tracks from the target and there is the (neutral) energy deposition in the electromagnetic calorimeter.

### *2.1. Charged pion Compton effect and polarizability*

The momentum transfer to the nuclei squared, $Q^2$, was calculated event by event from the kinematics of the measured initial and scattered pion and the radiated photon. With the parameters of this setup, the experimental accuracy of the momentum transfer squared, $Q^2$, typically of about $2 \times 10^{-4}$ GeV$^2/c^2$ was achieved for the reaction of pion radiative scattering. To select events belonging to this topology, as well as those likely scattered in the Coulomb field, the selection criteria were applied to the total energy of event, 35 GeV $< E_{\text{tot}} <$ 45 GeV, to check the energy conservation and the calculated momentum transfer squared, $Q^2 < 6 \times 10^{-4}$ GeV$^2/c^2$. Both distributions are shown in Fig. 2, *a* and *b*, respectively. They prove the completeness of the $\pi\gamma$ final state event topology and the scattering off the Coulomb field of the target nuclei.

The measurements were performed with different targets from carbon to lead (Fig. 3, *a*) to prove the expected $Z^2$ dependence of the cross section on the atomic number $Z$. In total, about 7000 events of pion Compton scattering were observed and reported in [8].

The main tool for the extraction of polarizabilities was found in [6] to be the energy $E_\gamma$ of the radiated photon. Since the most relevant models at the time predicted a zero value for the absolute magnitude of $\alpha_\pi + \beta_\pi$ or at least a value more than an order of magnitude smaller than the magnitude of $\alpha_\pi$ (which also holds true for modern predictions), it was decided to estimate the magnitude of $\alpha_\pi$ under the assumption that $\alpha_\pi + \beta_\pi = 0$. The relative contribution of the polarizability term to the differential over the radiated photon energy cross section significantly increased allowing for the relative measurement. The dependence of this term can be roughly

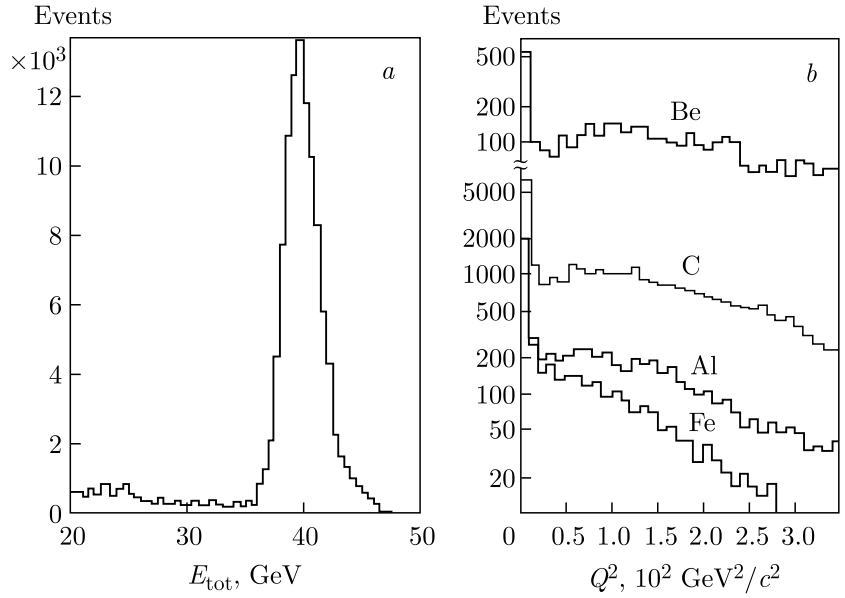


**Figure 2.** ($a$) Total energy of the final state pion and photon. ($b$) Distribution of events over the calculated momentum transfer squared, $Q^2$.

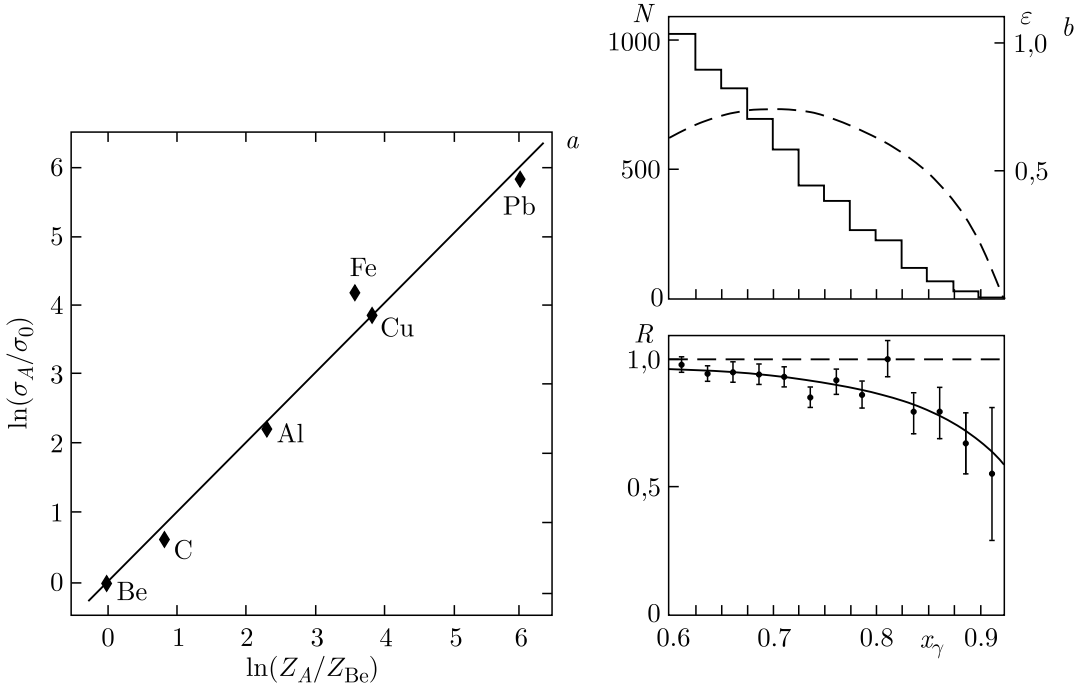


**Figure 3.** ($a$) $Z^2$-dependence of the cross section. ($b$) Top: the $x_\gamma = E_\gamma/E_{\text{beam}}$ distribution (left scale) and the $x_\gamma$-dependence of acceptance (right scale). Bottom: the measured cross section, normalized to the cross section of the point-like pion.

approximated by the following formula:

$$R_\pi(x_\gamma) = 1 - \frac{3}{2} \cdot \frac{x_\gamma^2}{1 - x_\gamma} \cdot \frac{m_\pi^3}{\alpha} \cdot \alpha_\pi, \tag{5}$$

where $x_\gamma = E_\gamma/E_{\text{beam}}$ and $R_\pi$ is the ratio of the cross section with an account of pion polarizability to the point-like pion cross section, $m_\pi$ is the pion mass, and $\alpha$ is the fine structure constant.

Formula (5) provides a simple demonstration of the functional behavior, but it should be noted that in the actual fitting procedure, the theoretical calculations which took into account higher-order QED, as well as some other corrections, were used. The uncertainty in these corrections and the difference of results obtained for different cut variations were included in the systematic error of the polarizability result.

The measurement performed using the full statistics of the experiment is shown in Fig. 3, *b*.

From this data sample, the value of the electric polarizability of the charged pion

$$\alpha_\pi = -\beta_\pi = (6.8 \pm 1.4_{\text{stat}} \pm 1.2_{\text{syst}}) \times 10^{-4}\ \text{fm}^3 \tag{6}$$

was obtained. Subsequently, the data was analyzed in [11] fitting electrical and magnetic polarizabilities separately, and this assumption was confirmed at the level of the accuracy of this experiment.

### *2.2.* $\gamma \to 3\pi$

When selecting events of another process under study, the pion pair production by pions, the same setup and the data sample were utilized [13]. However, in the reconstruction of photons, the fiducial volume of the calorimeter was extended to allow for an increase of acceptance of the photon pairs from the neutral pion decay. The reconstructed invariant mass $m_{\gamma\gamma}$ of two detected photons is shown in Fig. 4 for different nuclear targets. The events with an invariant mass of two photons from 0.09 to 0.17 GeV were selected for the further analysis.

The distribution of these events with the scattered and the neutral pions in the final state over their total energy $E_{\text{tot}}$ is shown in Fig. 5. A clear peak is observed in the total energy distribution at the nominal beam energy of 40 GeV.

The events with the total energy from 35 to 45 GeV were analyzed calculating their momentum transfered to the nucleus squared ($Q^2$). Those distributions are shown in Fig. 6 where one can observe the peak at small values, corresponding to the pion pair production by pions in the Coulomb field of the target nuclei.

The full cross section of this reaction was calculated for the kinematic range $Q^2 < 2 \times 10^{-3}$ GeV$^2/c^2$ and $m_{\gamma\gamma} < 10\ m_\pi^2$. The obtained value was found in agreement with theoretical calculations.

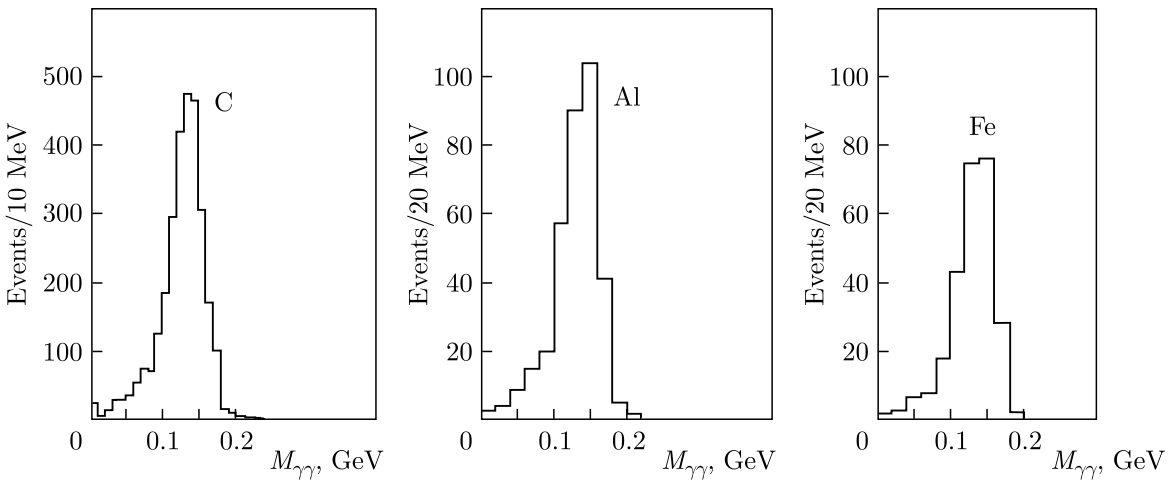


**Figure 4.** Invariant mass of two final state photons [13].

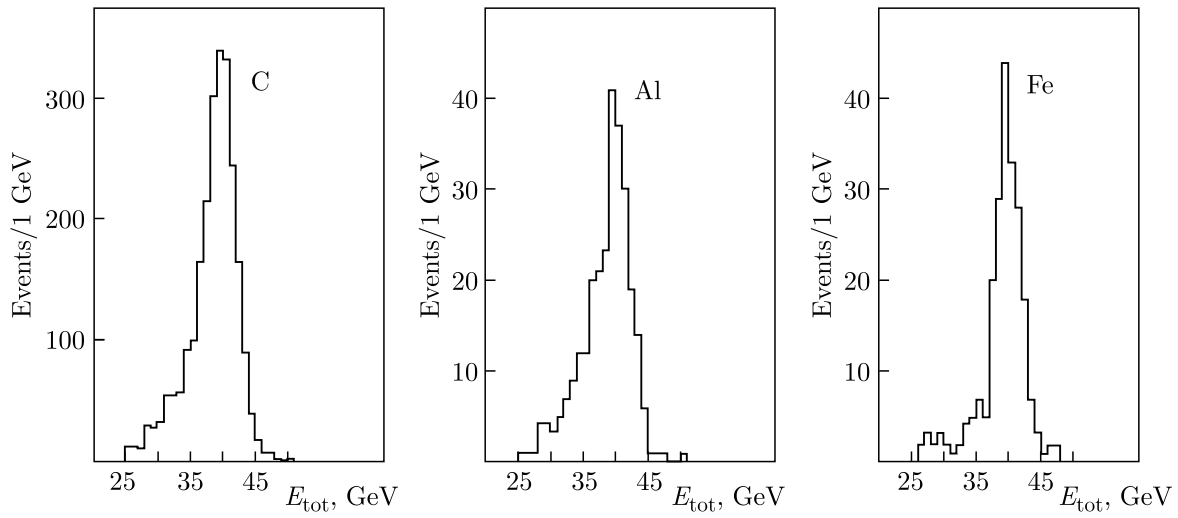


**Figure 5.** Total energy distribution of events [13].

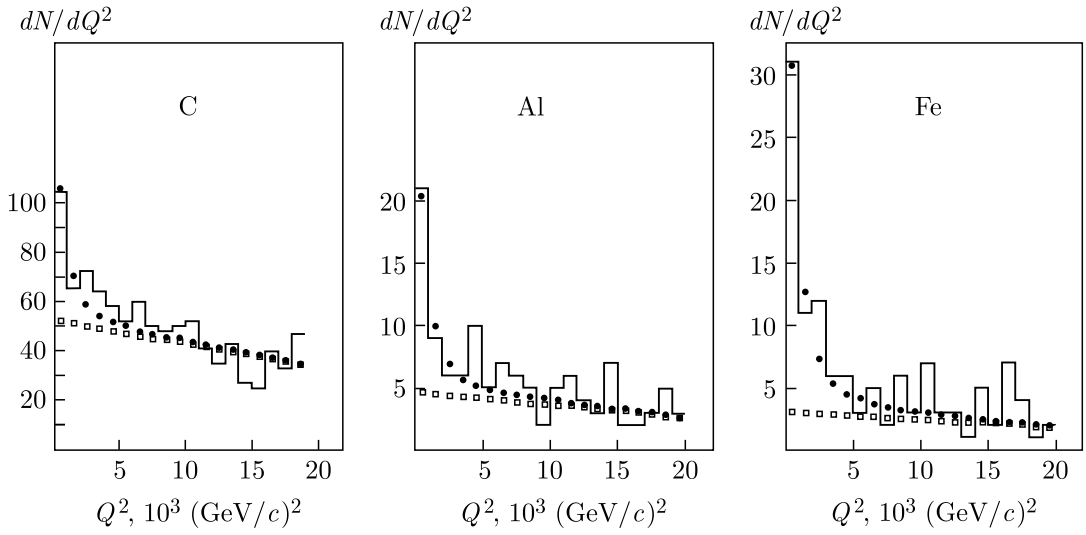


**Figure 6.** Distribution of events over the momentum transfer squared [13].

Extracting from the measured cross section the value of the $F_{3\pi}(0)$ constant which describes the $\gamma \to 3\pi$ vertex at the threshold, one can find [13]

$$F^{3\pi} = 12.9 \pm 0.9_{\text{stat}} \pm 0.5_{\text{syst}}\ \text{GeV}^{-3}. \tag{7}$$

The systematic uncertainty, coming from the extrapolation from the physical range of kinematic variables to $s = t = u = 0$, was estimated to be 1.0 GeV$^{-3}$. The obtained value is in agreement with the calculations based on the chiral anomaly hypothesis [14, 15].

## 3. Primakoff measurements with COMPASS (CERN)

### *3.1. COMPASS setup*

The study of strong interaction properties in the low-energy region through electromagnetic scattering of pions in the Coulomb field of a nucleus, including the measurement of the charged pion polarizabilities with a new level of precision, was continued in the COMPASS experiment at CERN.

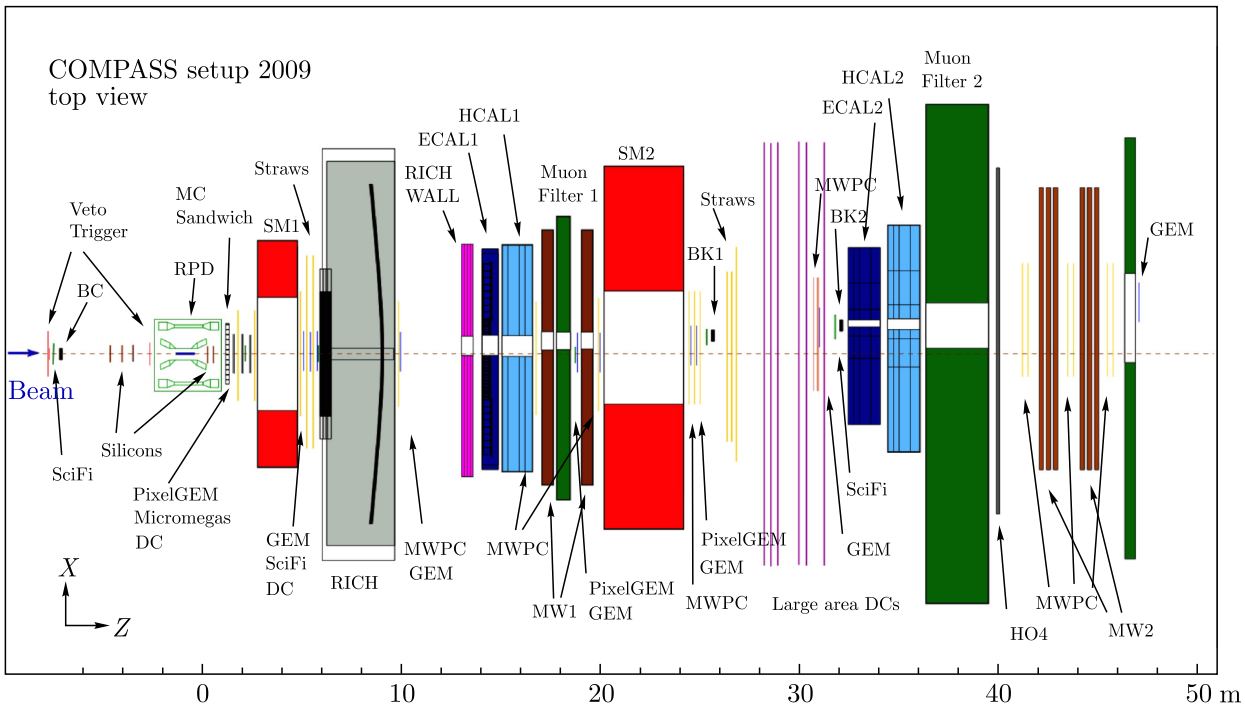


**Figure 7.** Top view of the COMPASS setup for data taking with hadron beams [18].

The COMPASS spectrometer at the secondary beam of the Super Proton Synchrotron, presented in Fig. 7, is a universal multipurpose setup developed to cover a wide range of physics tasks [17, 18]. For the Primakoff measurements with hard photons in the final state, the following elements of the setup were absolutely essential:

- the beam telescope, comprising three stations of silicon detectors located upstream of the nuclear target and two stations positioned downstream of the target; this configuration ensured the precise measurement of the pion's small scattering angle; the spatial resolution of these detectors was 4—11 $\mu$m, and their timing resolution was 1.4–1.8 ns;
- the small-angle aperture electromagnetic calorimeter ECAL2 which was responsible for the reconstruction of the photon cluster and served as a trigger element;
- the magnetic spectrometer, built around two spectrometric magnets SM1 and SM2, which enabled the measurement of the scattered pion momentum;
- the muon identification system MW2 which allowed for the filtering of the background caused by the muon component in the beam.

The negative hadron beam of 190 GeV/$c$ composed of 96.8% of pions, 2.4% of kaons, and 0.8% of antiprotons was used for data taking in the 2004, 2009, and 2012 Primakoff runs. The nominal intensity of the hadron beams was $5 \times 10^6$ s$^{-1}$. In addition to hadrons, a muon component was present on the level of about 1%, together with a negligibly small admixture of electrons. Two threshold Cherenkov detectors, CEDARs, were installed 30 m upstream of the target region to provide a fast beam particle identification for particle momenta. They were used for the kaon/pion separation.

The unique feature of the COMPASS experiment is the possibility to use use either the hadron beam or the muon beam of the same momentum with similar parameters. Since the

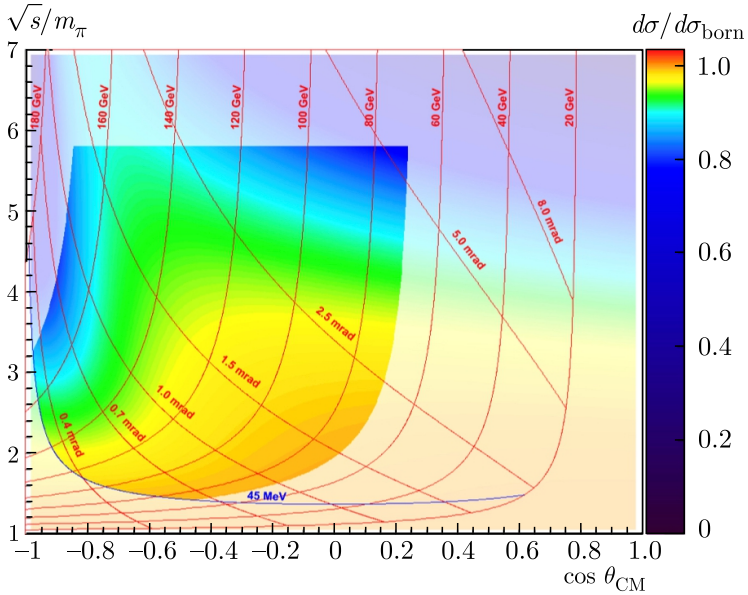


**Figure 8.** Relative effect of dipole polarizabilities (ChPT values) on the cross section as a function of the photon scattering angle and the energy for the system of the quasi-real photon and the pion in the center-of-mass system [19]. Red lines show the photon energy and the scattering angle in the laboratory system.

masses of the pion and the muon do not differ significantly, the kinematics of reaction (3) are also similar to the reaction

$$\mu^- + (A, Z) \to \mu^- + (A, Z) + \gamma. \tag{8}$$

Since the muon is a point-like structureless particle, the measured differential cross section $d\sigma_{\mu(A,Z)}/dx_\gamma$ for the muon should not differ from the theoretical prediction (although, of course, due to the difference in spins, the cross sections have different shapes for the pion and the muon). This allows the use of reaction (8) to check for possible systematic effects, which is an important advantage of the COMPASS experiment over the measurements performed in Serpukhov.

The kinematic range in terms of the photon scattering angle in the center-of-mass system, $\theta_{CM}$, and the center-of-mass energy, $\sqrt{s}$, for the system of the quasi-real photon and the pion covered by the COMPASS setup is shown in bright colours in Fig. 8. The colour scale illustrates a relative magnitude of the pion polarization effects [19]. For the detailed analysis of the kinematics see [20].

### *3.2. Pilot run 2004*

A two-week-long pilot data-taking run within the pion polarizability measurement programme was performed in the autumn of 2004. The primary target material was lead (3 mm). The copper (3.55 mm) and graphite (23.5 mm) targets were also used to study systematic effects and to verify the dependence of the Primakoff scattering cross section on the atomic number $Z$. During the run, the feasibility of the measurements, outlined in the experimental programme, was tested, and some conclusions were drawn in order to optimize the setup for subsequent measurements. Although the pilot run accumulated statistics of Primakoff $\pi\gamma$ events comparable to those gained in Serpukhov, an unfortunate oversight during the trigger installation led to significant uncontrolled systematic effects. The conclusions drawn from the results of the 2004 run served as the basis for preparing the new data taking in 2009. The detailed comparison of the data from the COMPASS Primakoff pilot run 2004 with the measurements obtained in Serpukhov is presented in [22].

### 3.3. Target selection for the main measurement

The main criteria for selecting the target material for studying Primakoff reactions were both the ratio between the rates of electromagnetic events and the events of the same configuration at low $Q^2$ values, produced via the strong interaction. If the number of the former is proportional in the Born approximation to the square of the target nucleus charge $Z$, then the number of the latter increases with the nucleus mass A approximately as $A^{2/3}$. The $Q^2$ distributions for lead, copper, and graphite targets, obtained during the 2004 run, are presented in Fig. 9, *a*. And Fig. 9, *b* shows the dependence of reaction cross section (3) on the target nucleus charge measured during the 2004 run. The dashed curve corresponds to the $Z^2$ dependence. On the basis of this criterion, it would be logical to use as a target a material with the maximum possible $Z$ value. It should be noted that the choice of graphite — a material with a low atomic number — as the main target in the Serpukhov experiment was driven by the concerns about an additional significant systematic uncertainty associated with the effects of excitation and disintegration of heavy target nuclei. These effects were subsequently not confirmed. However, the corrections to the Born cross section, as well as the associated systematic contribution to the measured value of the pion polarizability, increase in the absolute magnitude with the growth of the target nucleus charge. Fig. 10, *a* features the ratio of reaction cross section (3) — estimated taking into account radiative corrections at the Compton vertex, vacuum polarization, multiple photon exchange, screening of the nuclear charge by the electron shell, and the electromagnetic form factor of the target nucleus — to the corresponding Born cross section as a function of the target atomic number $Z$. Fig. 10, *b* shows the corresponding systematic contribution to the measured value of $\alpha_\pi$ under the assumption that $\alpha_\pi + \beta_\pi = 0$. Thus, for the lead target used as the main target in the 2004 run, the real cross section is reduced by 12% compared to the Born one, and the value of the pion electric polarizability $\alpha_\pi$, measured without an accurate account of the aforementioned corrections, would be $0.6 \times 10^{-4}$ fm$^3$, less than the true value.

As a compromise option for the 2009 run, a nickel target was chosen. The target thickness was also optimized, resulting in its reduction from about 0.5 $X_0$ to 0.3 $X_0$.

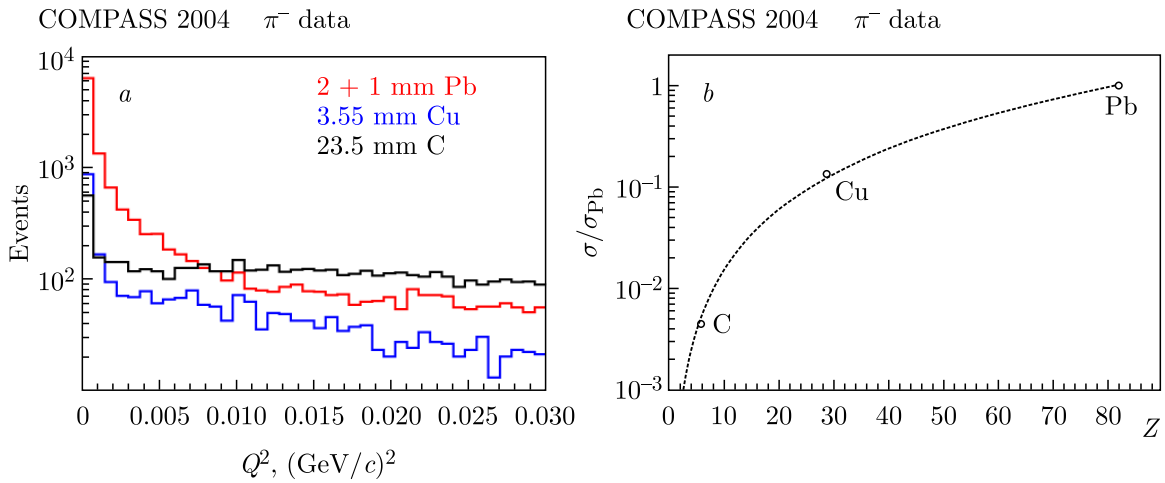


**Figure 9.** (*a*) Measured $Q^2$ distributions for the lead (red), copper (blue), and graphite (black) targets (pilot run 2004) [22]. (*b*) Measured dependence of reaction cross section (3) on the target atomic number (pilot run 2004). All cross section values are normalized to the corresponding value for lead. The dashed curve corresponds to a $Z^2$ dependence [22].

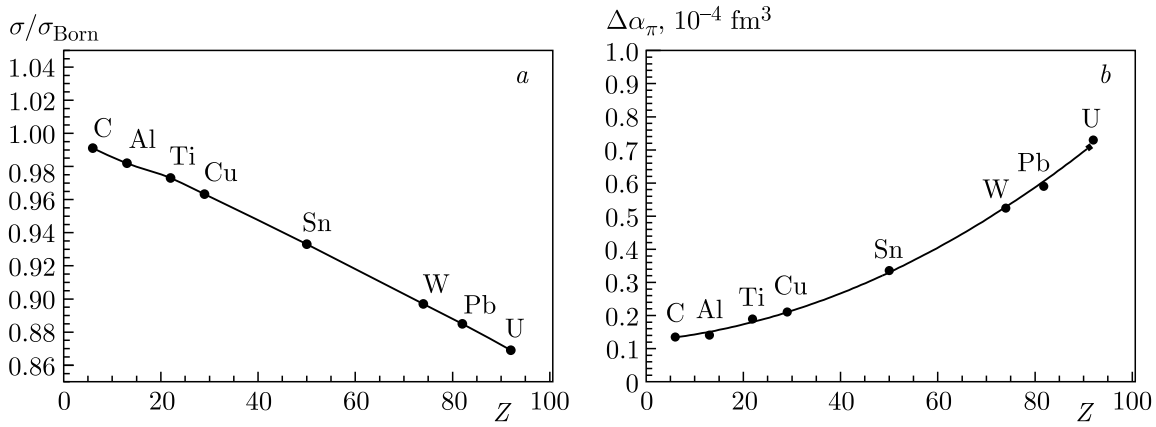


**Figure 10.** (*a*) Ratio of reaction cross section (3) — calculated with the account of radiative corrections at the Compton vertex, vacuum polarization, multi-photon exchange, screening of the nuclear charge by the electron shell, and the electromagnetic form factor of the target nucleus — to the corresponding Born cross section, as a function of the target nucleus atomic number $Z$. (*b*) Corresponding systematic contribution to the measured value $\alpha_\pi$ under the assumption that $\alpha_\pi + \beta_\pi = 0$ [22].

## 4. Polarizability extraction

The data used to extract the charged pion polarizabilities were collected during the 2009 run with a total duration of about one month. During the run, beams of negative pions and muons with a momentum of 190 GeV/$c$ were used alternately.

Figure 11, *a* shows the distribution of events in $|Q| = \sqrt{Q^2}$. The peak in the low $|Q|$ region with a width of about 12 MeV/$c$ corresponds to electromagnetic scattering, the following minimum — to the minimum of negative interference between electromagnetic scattering and the process with the same final state proceeding via the strong interaction, and the minimum around 0.17 GeV/$c$ — to the first diffraction minimum for the nickel nucleus. It should be noted that the observed width of the Coulomb peak is entirely determined by the experimental resolution, while its true width is at least an order of magnitude smaller. For the further analysis, events with $Q^2 < 1.5 \times 10^{-3}$ (GeV/$c$)$^2$ were used. We have to mention that the small background of events caused by the strong interaction, as well as the interference term, is also present under the Coulomb peak. The Monte Carlo electromagnetic data are shown for the reference. To eliminate the significant background from the intermediate $\rho^-(770)$ production

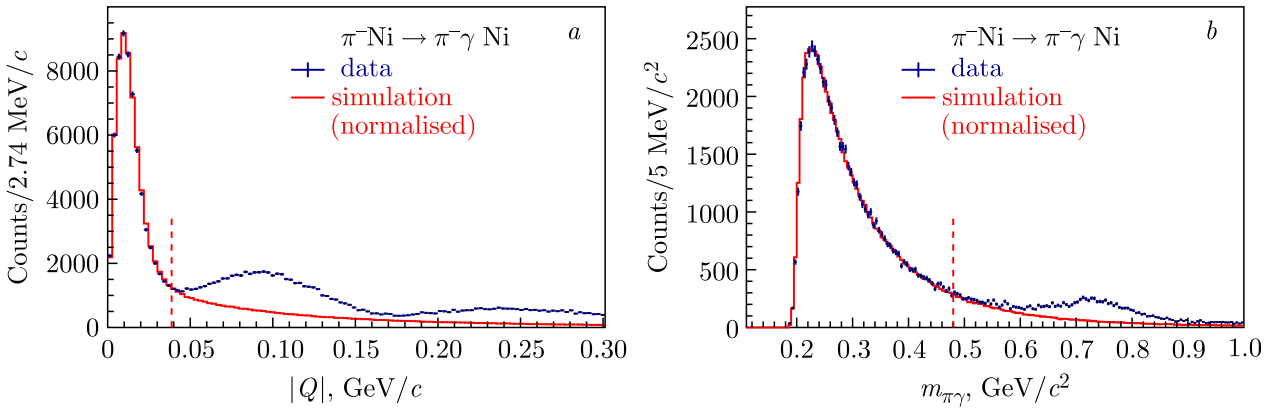


**Figure 11.** Comparison of the measured (black dots with errors) and numerically simulated (red histograms) distributions for the measurements with the pion beam: (*a*) for the modulus of the 4-momentum transfer to the nucleus $|Q|$ [23]; (*b*) for the invariant mass of the final state $m_{\pi\gamma}$. The values of the selection criteria are indicated by the red vertical dashed line [23].

with its subsequent decay into $\pi^-\pi^0$, only events with $m_{\pi\gamma} < 3.5m_\pi \approx 0.487$ GeV/$c^2$ were considered, as shown in Fig. 11, *b*.

To study polarization effects, the region $0.4 < x_\gamma < 0.9$ was chosen due to the constant trigger efficiency and to the stably high efficiency for identifying scattered muons. This region corresponds to the range $-1 < \cos\theta_{CM} < 0.15$ in the CMS system that is sensitive to the value of $\alpha_\pi - \beta_\pi$. The final number of the events available for extracting the pion polarizability was 63,000.

The extraction of the pion polarizabilities was performed under the assumption that $\alpha_\pi + \beta_\pi = 0$. In addition to the Born term, the following corrections to the cross section were taken into account in the numerical simulation: radiative corrections [24–26], chiral loop corrections [27], and the correction for the electromagnetic form factor of the nickel nucleus, calculated under the approximation treating the nucleus as a sphere of the radius $r = 5$ fm: $F(Q^2) = j_1(rq)$, where $q$ is the magnitude of the 3-momentum transferred to the nucleus.

The combined effect of the aforementioned corrections on the event distribution in $x_\gamma$, expressed as a correction to the measured value of $\alpha_\pi$, was $+0.6 \times 10^{-4}$ fm$^3$. The ratio $R_\pi$ of the measured differential cross section $d\sigma_{\pi\gamma}/dx_\gamma$ to the expected cross section for a point-like scalar particle (taking into account the corrections stated above) is shown in Fig. 12, *a*. The value of the electric polarizability $\alpha_\pi = (2.0 \pm 0.6_{\text{stat.}}) \times 10^{-4}$ fm$^3$ was obtained from the fit of the function $R_\pi(x_\gamma)$ (5) to the experimental data points in the interval $0.4 < x_\gamma < 0.9$. The fit used two free parameters: the electric polarizability $\alpha_\pi$ and the overall normalization factor (effectively, the integrated luminosity was achieved in the experiment). The quality of the fit can be characterized by a $\chi^2$/NDF value of 22.0/18.

To check for the absence of unaccounted systematic effects, the analysis was repeated for the data collected with the muon beam of the same energy and similar intensity. For this purpose, all the same selection criteria that were used for the pion data were applied to the muon data, except for the upper limit on the mass of the final state — it was changed from $3.5m_\pi$ to $3.5m_\mu$. The simulation also accounted for radiative corrections [24, 28] and corrections for the form factor of the nickel nucleus. Although, due to the different spin, the shapes of the $x_\gamma$ distributions for $\pi\gamma$ and $\mu\gamma$ events differ significantly, the measured differential cross section $d\sigma_{\mu\gamma}/dx_\gamma$ must exactly match that predicted by QED. The measured ratio $R_\mu$, shown in Fig. 12, *b*, corresponds to the 'false' polarizability of $(0.5 \pm 0.5_{\text{stat.}}) \times 10^{-4}$ fm$^3$ obtained from fitting function (5) to the measured ratio $R_\mu$. Special attention should be paid to the fact that expression (5) uses the pion mass, not the muon one. For this fit, $\chi^2/NDF = 19.6/18$. The obtained value of the 'false' polarizability agrees within the error with zero, indicating the absence of significant unaccounted contributions to the systematic uncertainty.

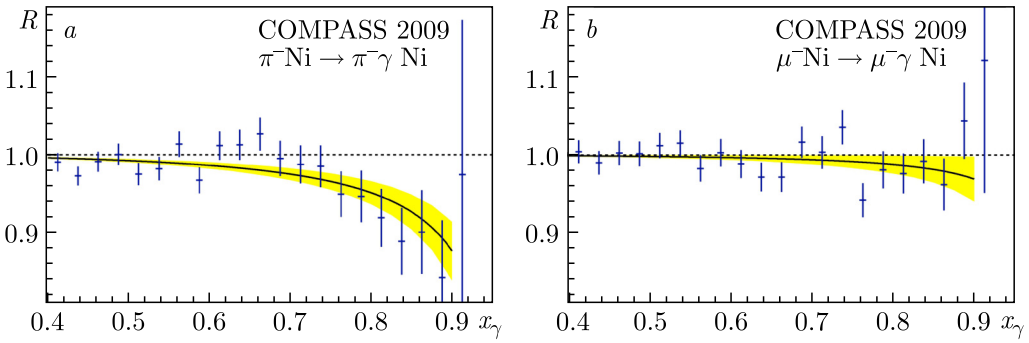


**Figure 12.** $x_\gamma$ dependence of the ratio of the measured differential cross section $d\sigma/dx_\gamma$ to that expected for the point-like pion (*a*) and muon (*b*). The fit result is shown by the black curves, and the error band corresponding to one standard deviation is shown by the yellow area [23].

## 5. Systematic effects

Regarding the estimation of the systematic measurement error, it was found that the main contributions are:

- the uncertainty associated with the limited accuracy of determining the tracking detector efficiency incorporated into the simulation;
- the uncertainty associated with the fact that the simulation does not account for Coulomb corrections [30], as well as corrections for multi-photon exchange [31] and the effect of partial shielding of the nuclear charge by the electron shell;
- the statistical uncertainty of the $\pi^0$ background subtraction;
- the uncertainty associated with the influence of the strong interaction background and its interference with the Coulomb interaction on the shape of the $x_\gamma$ distribution;
- the contribution from the process of elastic scattering of beam pions off atomic electrons in which the scattered electron emits the hard photon in the target material and then gets lost;
- the contribution from the process $\mu^- + Ni \to \mu^- + Ni + \gamma$ in which the scattered muon is misidentified as a pion.

To study the influence of the strong interaction background, a fit of an empirical function describing the shape of the $Q^2$ distribution which included a Coulomb term, a diffractive term, and their interference was applied to the experimental data. It should be noted that the interference term is negative, which is in agreement with the expectation [32]. The results of the fit in different $x_\gamma$ intervals agree within statistical errors, which allowed one to estimate the corresponding contribution to the systematic error.

To estimate the background from the small admixture of electrons present in the hadron beam, part of the data was taken with an electron converter installed in the beam channel, which was an additional lead target. It was found that the background from electron bremsstrahlung is effectively suppressed by the selection of the transverse momentum of the charged particle and is ultimately negligible compared to other background sources.

The estimates of each of the contributions are given in Table 1. The total systematic error was obtained by quadratic summation of all contributions. Taking it into account, the

**Table 1.** Estimation of the main contributions to the systematic error of the $\alpha_\pi$ measurement under the assumption that $\alpha_\pi + \beta_\pi = 0$.

| Source of systematic error | Estimate of contribution, $10^{-4}$ fm$^3$ |
|---|---|
| Determination of tracking detector efficiency | 0.5 |
| Radiative corrections | 0.3 |
| $\pi^0$ background subtraction | 0.2 |
| Strong interaction background estimation | 0.2 |
| Elastic $\pi e$ scattering | 0.2 |
| Muon component of the beam | 0.05 |
| Quadratic sum | 0.7 |

final result for the electric polarizability of the pion $\alpha_\pi$, obtained under the assumption that $\alpha_\pi + \beta_\pi = 0$, is as follows:

$$\alpha_\pi = (2.0 \pm 0.6_{\text{stat.}} \pm 0.7_{\text{syst.}}) \times 10^{-4} \text{ fm}^3. \quad (9)$$

The possible influence of contributions from higher-order terms in the expansion of the Compton amplitude near the threshold was investigated by varying the upper limit of the selection of the final state mass in the range from 0.40 GeV/$c^2$ to 0.57 GeV/$c^2$. As a result, no substantial impact was found.

More details on this measurement can be found in [21].

## 6. Discussion of the results and plans for measuring pion polarizabilities

All available experimental results for the difference of the charged pion polarizabilities, obtained under the assumption that $\alpha_\pi + \beta_\pi = 0$, including the result from the COMPASS experiment, are presented in Fig. 13, *a*. A summary of the results from four dedicated measurements, including the COMPASS measurement, is given in Fig. 13, *b*.

The result on the charged pion polarizabilities obtained in the COMPASS experiment is in good agreement with the predictions of the Chiral Perturbation Theory, which is undoubtedly an important fact confirming the status of this model as the most successful one in the low-energy region. Furthermore, the obtained result can be used to refine the values of low-energy constants. Also, it does not contradict the currently available preliminary results from lattice QCD calculations in [33, 34, 37] and [35], the latter being based on the preceding consideration of neutral mesons [36].

As it was mentioned above, approximate formula (5) is not used directly for data treatment. However, a number of corrections are additionally applied considering different effects. The main publication [23] explicitly mentions various corrections accounted for at the level of the simulation and the systematic error estimation. In particular, this concerns higher-order QED corrections, the contribution of strong interaction, and the interference term, as well as some other effects advocated by [38, 39].

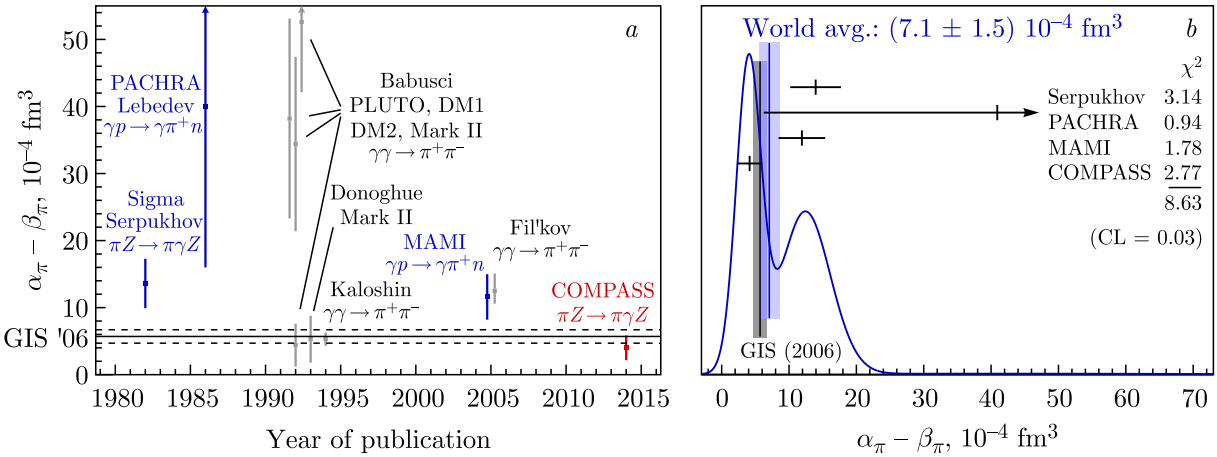


**Figure 13.** (*a*) Experimental results on the value $\alpha_\pi - \beta_\pi$ from various sources, sorted by the publication year, including the COMPASS result (shown in red). The results from previous dedicated experiments are shown in blue. The prediction of the Chiral Theory [16] and its uncertainty are shown by the solid and dashed horizontal lines, respectively [29]. (*b*) Summary of the results on the value $\alpha_\pi - \beta_\pi$ obtained in dedicated experiments, including COMPASS (the result shown in red) [29]. The weighted average value is shown by the vertical blue line, and its error by the blue rectangle. The prediction of the Chiral Theory [16] is shown by the gray rectangle.

With the experience from the 2009 run in mind, the COMPASS experiment took data in order to measure the charged pion polarizability in 2012. The accumulated statistics for the corresponding $x_\gamma$ range were several times higher than in 2009. The detailed information on the modification of the setup prior to the 2012 run can be found in [40]. From the analysis of these data one could expect the result for the polarizability $\alpha_\pi$ under the assumption that $\alpha_\pi + \beta_\pi = 0$ with an accuracy a few times better than the published result. Furthermore, independent measurements of the values $\alpha_\pi + \beta_\pi$ and $\alpha_\pi - \beta_\pi$ are possible with the accuracy of the sum of the polarizabilities anticipated to be smaller than the value predicted by the Chiral Theory ($0.16 \times 10^{-4}$ fm$^3$) [16]. However, in order to cope with the theory at this level, it is also necessary to minimize the values of experimental systematic errors. The most critical ones, such as those related to the detector effects, the strong background contribution, and the $\pi^0$ background subtraction, can be significantly reduced due to the increased statistics. Additionally, radiative corrections can be calculated at a higher level of accuracy.

The proposal to use a previously unexploited process of photoproduction of a charged pion pair on a nuclear target for the precision measurement of the charged pion polarizability was expressed in [41, 42] using the GlueX experimental setup in JLab. A 12 GeV electron beam from the CEBAF accelerator was proposed as a source of high-energy photons. A secondary photon beam with an energy of 5.5–6 GeV, an intensity of $10^7$ s$^{-1}$, and a degree of linear polarization up to 76% was planned to be directed onto a $^{116}$Sn target with a thickness of 0.6 mm, although other options were also discussed.

The planned accuracy for measuring the value of $\alpha_\pi - \beta_\pi$ was estimated to be of about $0.6 \times 10^{-4}$ fm$^3$. The main source of the background was apparently the coherent production of $\rho^0(770)$ with its subsequent decay into $\pi^+\pi^-$. It was expected that the contribution of this background could be accounted for by analyzing the azimuthal distributions in the pion pair production. Furthermore, the production of lepton (especially muon) pairs in the Coulomb field of the target nucleus posed a certain risk.

The data were accumulated within the CPP experiment in 2022 [43]. Approximately $10^{11}$ triggered events were recorded with the lead target, and $2.3 \times 10^{10}$ triggered events with the empty target for background subtraction. The expected accuracy of the cross section measurement is shown in Fig. 14.

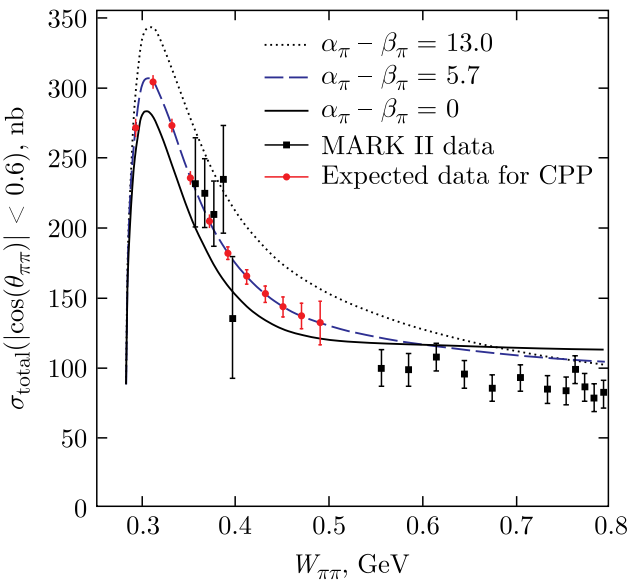


**Figure 14.** Cross section of the $\gamma\gamma \to \pi^+\pi^-$ process as a function of the center-of-mass energy. The solid, dashed, and dotted curves are derived from calculations using the dispersion model with $\alpha_\pi - \beta_\pi$ equal to 0.0, $5.7{\times}10^{-4}$ fm$^3$ (ChPT), and $13.0{\times}10^{-4}$ fm$^3$, respectively. The black data points are from the MarkII experiment while the red data points are the expected data points for the CPP experiment [43, 44].

## 7. Tests of predictions of the chiral anomaly

### 7.1. Measurement of the $\gamma \to 3\pi$ coupling constant

In 2022, the COMPASS collaboration revealed preliminary results on the measurement of the $F_{3\pi}$ constant which describes the $\gamma \to 3\pi$ vertex [45] using reaction (4). The elements of the production mechanism of this reaction were already studied in [46].

The COMPASS analysis represents a significant improvement on the SIGMA collaboration result as it uses the dispersive framework described in [47]. This dispersive framework takes into account the two production mechanisms of the process under study: the resonant $\rho$-meson production and the effective four-point coupling, governed by the chiral anomaly, see Fig. 15. This allows one to utilize the data with the invariant $\pi^-\pi^0$ mass up to about 1 GeV/$c^2$. Fig. 16 shows the two contributions and their coherent sum to the cross section. The information on the contribution of the chiral anomaly can therefore be also extracted from the shape of the shifted $\rho$-meson peak while in Serpukhov only the near-threshold region far from the $\rho$-meson peak was used.

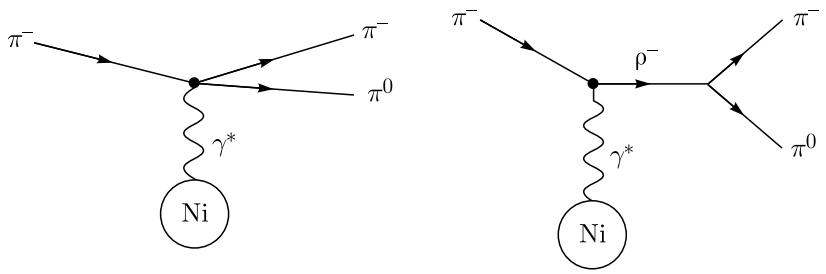


**Figure 15.** Production mechanisms of the $\pi\pi$ final state in the pion–photon interaction.

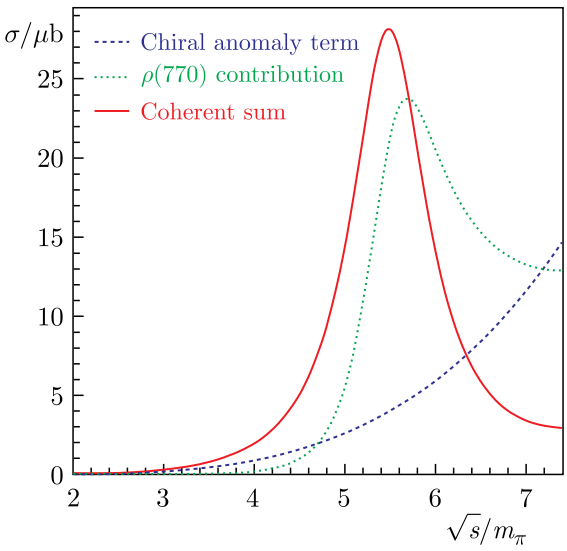


**Figure 16.** Conceptual plot of contributions to the $\pi\gamma \to \pi\pi$ cross section, calculated using a simplified tree-graph model [48].

The analysis was performed using the 2009 Primakoff dataset. About 105,000 events with $\pi^-\pi^0$ in the final state fulfilling the energy balance requirement were selected with the squared momentum transfer $Q^2 < 1.3 \times 10^{-3}$ GeV$^2$/c$^2$.

For the process under study, the dominant background source is the diffractive production of $\pi^0\pi^0$. Unlike the production of a single $\pi^0$, this process can occur via the Pomeron exchange, and therefore has a much higher cross section. The background $\pi^-\pi^0\pi^0$ events can be detected as $\pi^-\pi^0$ signal events if one of the neutral pions has a low energy and its decay photons are not detected with the electromagnetic calorimeter. Understanding this background is therefore vital for a precision measurement of $F_{3\pi}$. The Monte Carlo sample for the diffractive background $\pi^-\pi^0\pi^0$ was obtained from the separate dedicated partial wave analysis of the $3\pi$ final state.

To separate the signal events from the background and to determine the number of the Primakoff $\pi^- + \mathrm{Ni} \to \mathrm{Ni} + \pi^- + \pi^0$ events as a function of the two-pion system mass $M_{2\pi}$, the

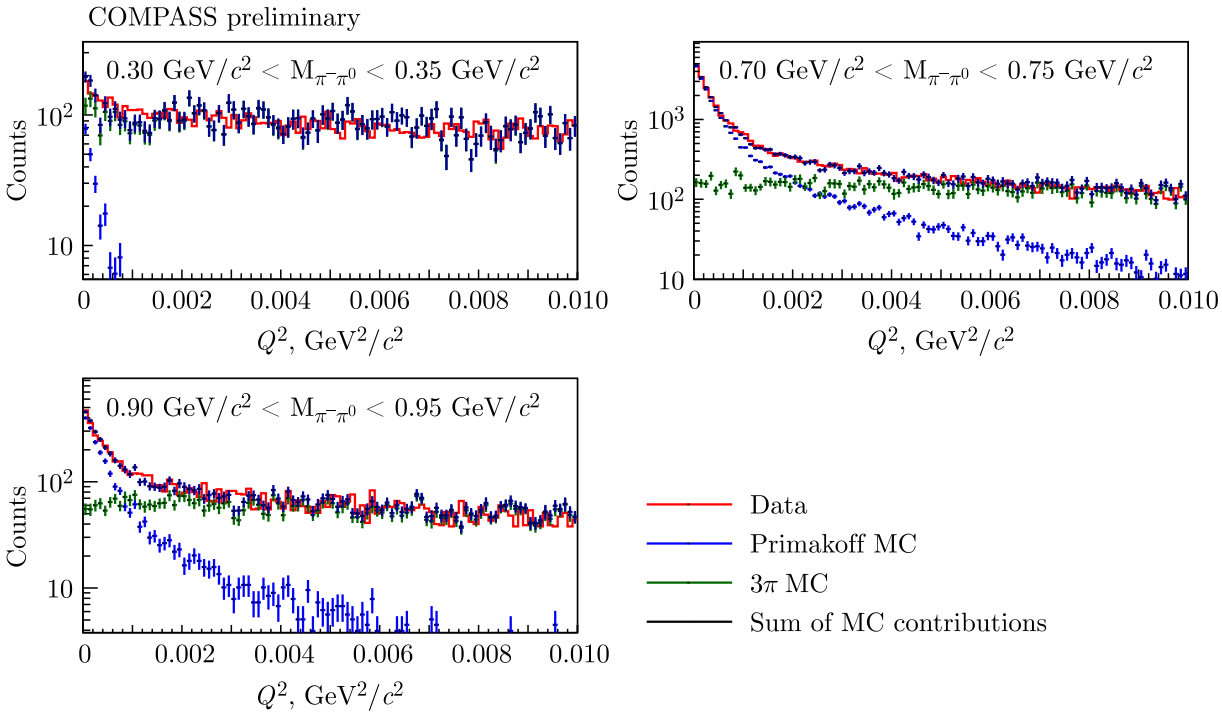


**Figure 17.** $Q^2$ of the selected data distributions with a sum of the signal and diffractive background Monte Carlo samples in the two-pion mass bins. Taken from [45].

$Q^2$ fits of the data distribution with the sum of the signal and the background Monte Carlo sample were performed, see 17.

To normalize the obtained mass-dependent distribution and to obtain absolute cross section values, the kaon decay events with the same final state, $\pi^-\pi^0$, where the kaon decayed outside the target, were analyzed. Using the knowledge of the kaon-to-pion beam particle ratio and the acceptance-corrected number of the detected kaon decays, the integral beam pion flux and subsequently the cross section of the signal process were measured.

In the final step of the analysis, the extraction of the $F_{3\pi}$ coupling constant, the differential cross section of the $\pi^- + \mathrm{Ni} \to \mathrm{Ni} + \pi^- + \pi^0$ was fitted with a two-parameter theoretical cross section distribution from the dispersive framework of [47], see Fig. 18, *a*. On the one hand, these two parameters are the subtraction constants arising in the calculation of the amplitude from the $\pi\pi$ phase shift. On the other hand, the calculation in the Chiral Perturbation Theory involves both the value of $F_{3\pi}$ at $s = t = u = 0$ and its expansion to the physical region. By matching the dispersive treatment with the calculation in the Chiral Perturbation Theory, the preliminary value of $F_{3\pi}$ at $s = t = u = 0$ GeV$^2$ was obtained:

$$F_{3\pi} = 10.3 \pm 0.1_{\mathrm{stat}} \pm 0.6_{\mathrm{syst}}\ \mathrm{GeV}^{-3}. \tag{10}$$

As the dispersive model takes into account the resonant production of the $\pi\pi$ system featuring the $\pi\gamma \to \rho$ vertex, it is possible to simultaneously obtain the radiative decay width of the $\rho$-meson, $\rho \to \gamma\pi$ [45]:

$$\Gamma_{\rho\to\pi\gamma} = 76 \pm 1_{\mathrm{stat}}\, {}^{+10}_{-8\,\mathrm{syst}}\ \mathrm{keV}. \tag{11}$$

To date, the COMPASS measurement is the most precise measurement of the $F_{3\pi}$ constant. It is also a combined measurement of $F_{3\pi}$ and $\Gamma_{\rho\to\pi\gamma}$. The compilation of the experimental results and the comparison with the chiral anomaly prediction are shown in Fig. 18, *b*.

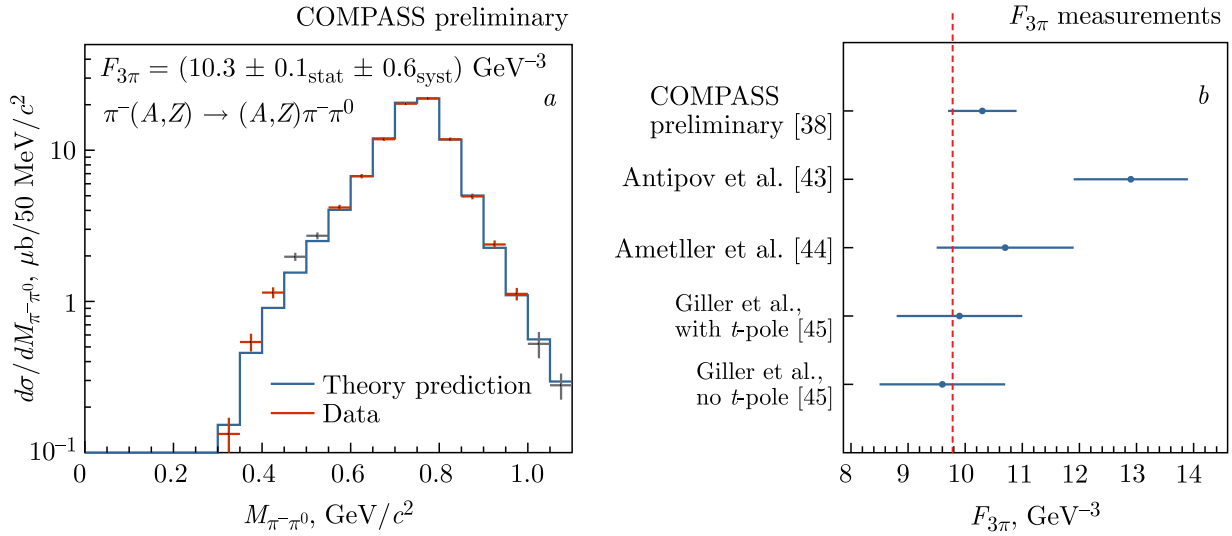


**Figure 18.** (*a*) Fit of the measured $\pi^- + \text{Ni} \to \text{Ni} + \pi^- + \pi^0$ cross section with the dispersive model from [47]. (*b*) Compilation of the experimental results on the $F_{3\pi}$ constant and the comparison with the chiral anomaly prediction (dashed vertical red line). References: [45, 49–51].

The analysis is currently being finalized by the COMPASS collaboration with the aim to significantly reduce the systematic uncertainty.

### *7.2. Chiral anomaly measurements in the $\pi\gamma \to \eta\pi$ process*

In general, the chiral anomaly and the Wess–Zumino–Witten term [14, 15] yield coupling strengths for the interactions involving the odd number of pseudoscalar bosons which includes, besides $\gamma \to 3\pi$, also the $\pi\gamma \to \eta\pi$ and $K\gamma \to K\pi$ processes. It is therefore of interest to test chiral anomaly predictions also for heavier pseudoscalar bosons.

The chiral anomaly yields the prediction for the coupling strength of the $\pi\gamma \to \eta\pi$ vertex: $F_{\eta\pi\pi\gamma} = 5.65 \pm 0.03$ GeV$^{-3}$.

Unlike in the case of the $\pi\gamma \to \pi\pi$ vertex, the $\eta\pi$ final state can be produced diffractively, mainly via the resonant production of $a_2(1320)$.

The VES collaboration attempted to measure the value of $F_{\eta\pi\pi\gamma}$ which corresponds to the $\pi\gamma \to \eta\pi$ vertex [52]. From the fit of the $Q^2$ distributions, the $N_{Primakoff} = 109 \pm 23$ Primakoff events were reconstructed in the kinematic range of $m_{\eta\pi} < 1.18$ GeV and $|Q^2 - Q^2_{\text{min}}| < 0.09$ GeV$^2/c^2$, which led to the measured value: $F_{\eta\pi\pi\gamma} = 6.9 \pm 0.7$ GeV$^{-3}$. There, $Q_{\text{min}} = \frac{s - m_\pi^2}{2p_{\text{beam}}}$ is the minimum momentum transfer to the nucleus, $s$ is the squared center-of-mass energy of the final state $\pi\eta$ system, and $p_{\text{beam}}$ is the beam particle momentum.

A theoretical framework was developed [53] for analyzing the $\eta\pi$ final state which provides a combined description of the direct 4-point anomalous coupling and the resonant production of the $a_2$-meson. There are plans to analyze the COMPASS Primakoff data using the mentioned theoretical description with the goal of testing the chiral anomaly prediction with the process involving the $\eta$-meson.

## 8. On the possibility of measuring the polarizability of the charged kaon in AMBER

The kaon, being a Goldstone boson in the SU(3) Symmetric Chiral Theory, is as fundamental an object of QCD as the pion. Since the charged kaon is a more compact object than the charged pion (their charge radii are $0.659 \pm 0.004$ and $0.560 \pm 0.031$ fm, respectively [54]), it would be logical to expect a smaller polarizability value for the kaon than for the pion.There was long

since a number of theoretical calculations of the pion and kaon polarizabilities performed using the chiral approach, see in [55–57], and in one of the relatively recent papers [58] that uses the Chiral Perturbation Theory and gives the following prediction for the polarizabilities of the charged kaon:

$$\alpha_K + \beta_K \approx 0, \quad \alpha_K = (0.64 \pm 0.10) \times 10^{-4} \text{ fm}^3 \tag{12}$$

Similar results were obtained within the domain model of the QCD vacuum [59]. The prediction of the quark confinement model [60] is

$$\alpha_K + \beta_K = 1.0 \text{ fm}^3, \quad \alpha_K = (2.3 \pm 0.10) \times 10^{-4} \text{ fm}^3 \tag{13}$$

that differs noticeably from the prediction of the Chiral Perturbation Theory (10). The lattice calculations are already bearing their first fruits, but the result remains quite uncertain [61]. As for the experimental data, currently, there is only an upper limit for the polarizability of the charged kaon

$$\alpha_K < 200 \times 10^{-4} \text{ fm}^3 \ (CL = 90\%), \tag{14}$$

obtained from the analysis of the X-ray spectrum of kaonic atoms [62].

The experience gained from working with the kaon component of the hadron beam during the 2008, 2009, and 2012 runs showed that measuring the kaon polarizability in the COMPASS experiment conditions in the process

$$K^- + (A, Z) \to K^- + (A, Z) + \gamma \tag{15}$$

using the standard hadron beam is an extremely difficult task. This kind of measurements is complicated by the following factors:

- the fraction of kaons in the beam is small;
- the cross section of the electromagnetic radiative scattering of the kaon off the target nucleus is $(m_K/m_\pi)^2 \approx 12$ times smaller than that of the pion;
- the efficiency and the purity of the beam kaon identification by CEDAR Cherenkov detectors are insufficient for confident registration of the effects related to the kaon polarizability.

Separately, it should be noted that in the case of the kaon, the kinematic range of invariant masses of the final state between the threshold and the first excited state $K^*(892)$ (taking into account that the width $\Gamma^*$ of this state is $\sim m^* - \Gamma^*$), expressed in units of the incident particle mass, is much smaller than in the case of the pion and $\rho^-(770)$. Thus,

$$(m_{K^*(892)} - \Gamma_{K^*(892)})/m_K - 1 = 0.7, \tag{16}$$

while for the pion

$$(m_\rho - \Gamma_\rho)/m_\pi - 1 = 3.4. \tag{17}$$

The impact of the $K^*(892)$ resonance on the result of the kaon polarizability measurement is discussed in [63].

Therefore, although COMPASS has about 1,000 events of process (15) recorded on tape in the 2009 and 2012 runs, it is unlikely that they will be used to estimate the kaon polarizability. However, if the reliability of the beam kaon identification can be improved in the future, the measurements could be repeated within a new project.

Currently, there is an active discussion about creating an intense kaon-enriched beam (up to $2 \times 10^7$ s$^{-1}$) at CERN on the basis of the radiofrequency separation technology of the AMBER project, the successor to the COMPASS experiment. This modification provides a unique opportunity to precisely measure the charged kaon polarizability for the first time [64, 65]. The following data-taking conditions were considered:

- the $K^-$-beam with a momentum of 100 GeV/$c$ and an intensity of $5 \times 10^6$ kaons per second;
- the spectrometer configuration similar to the one used in the COMPASS experiment for analogous measurements with the pion beam: CEDAR detectors for beam particle identification, the thin nickel target with a thickness of 0.3 $X_0$, a set of silicon tracking detectors positioned upstream and downstream of the target;
- the trigger for the energy deposition in the electromagnetic calorimeters ECAL1 and ECAL2;
- the new data acquisition system capable of accepting up to $10^5$ events per second.

Assuming that the total number of kaons delivered to the target is $5 \times 10^{12}$ (which roughly corresponds to one year of data taking) and the trigger efficiency is close to 100%, one can expect up to $6 \times 10^5$ Primakoff $K\gamma$ events in the kinematic range $0.1 < x_\gamma < 0.6$ and $M_{K\gamma} < 800$ MeV/$c^2$. The expected event distribution in $x_\gamma$ is shown in Fig. 19, *a*. By analogy with formula (5), the ratio $R_K$ of the differential cross section of process (15) for the real kaon to the corresponding cross section for the point-like structureless kaon as a function of $x_\gamma$, under the assumption that $\alpha_K + \beta_K = 0$, can be written as:

$$R_K(x_\gamma) = 1 - \frac{3}{2} \cdot \frac{x_\gamma^2}{1 - x_\gamma} \cdot \frac{m_K^3}{\alpha} \cdot \alpha_K. \tag{18}$$

It should be noted that polarization effects for the kaon, for the same values of polarizabilities, are $(m_K/m_\pi)^3 \approx 44$ times larger than those for the pion. Fig. 19, *b* shows the behavior of the

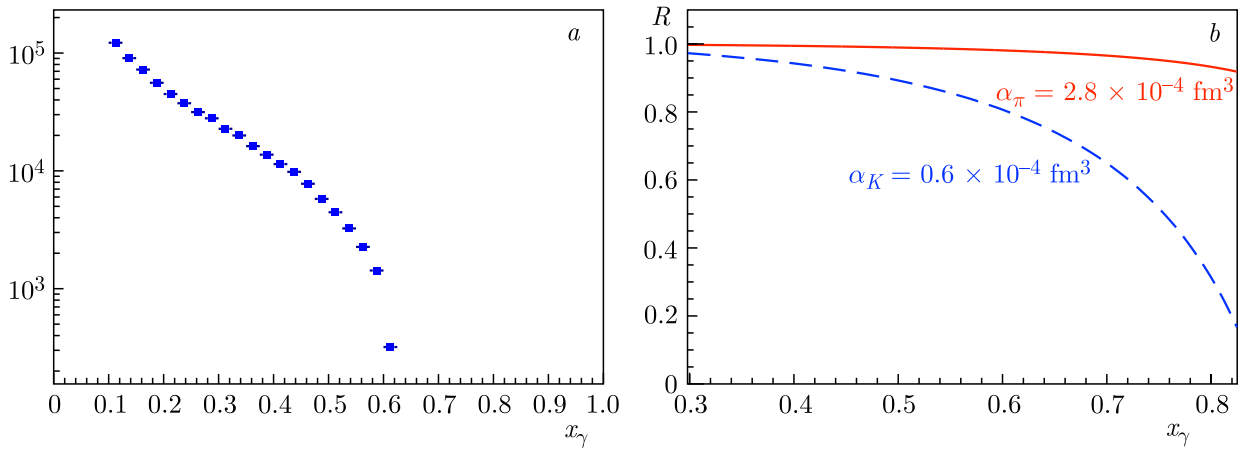


**Figure 19.** (*a*) Expected distribution of Primakoff $K^-\gamma$ events in $x_\gamma$ for $M_{K\gamma} < 800$ MeV/$c^2$ [65]. (*b*) Ratios $R_\pi$ (shown by the solid red line) and $R_K$ (shown by the blue dashed line) for the values of the polarizabilities $\alpha_{\pi,K}$ predicted by the Chiral Theory as functions of $x_\gamma$ under the assumption that $\alpha_{\pi,K} + + \beta_{\pi,K} = 0$ [64].

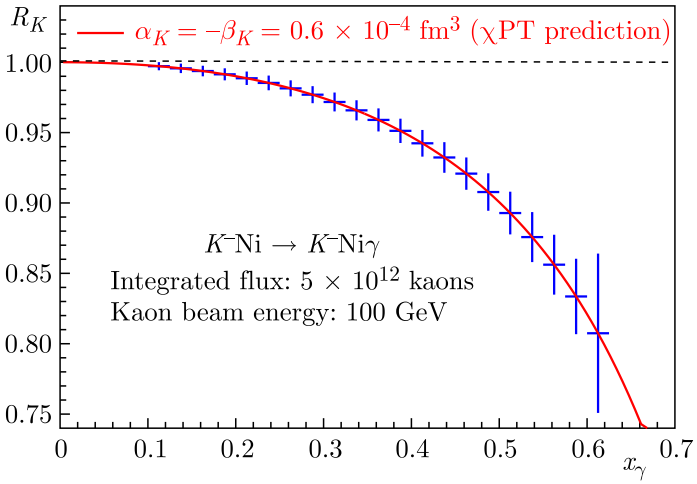


**Figure 20.** Expected statistical accuracy of the $R_K$ ratio measurement under the assumption that $\alpha_K + \beta_K = 0$. The behavior of the $R_K$ ratio predicted by the Chiral Theory is shown by the red curve [65].

ratios $R_\pi$ and $R_K$ for the values of the polarizabilities $\alpha_{\pi,K}$ predicted by the Chiral Theory as functions of $x_\gamma$ under the assumption that $\alpha_{\pi,K} + \beta_{\pi,K} = 0$.

The expected statistical accuracy of the $R_K$ ratio measurement is shown in Fig. 20. The red curve corresponds to the value of the kaon polarizability $\alpha_K$ predicted by the Chiral Theory. The corresponding statistical accuracy for extracting the value of $\alpha_K$, under the assumption that $\alpha_K + \beta_K = 0$, is $0.03 \times 10^{-4}$ fm$^3$. As for the systematic uncertainty, the following main contributions are expected:

- the uncertainty associated with the limited accuracy of determining the tracking detector efficiency used in the simulation;
- the statistical uncertainty of the $\pi^0$ background subtraction;
- the uncertainty associated with the influence of the strong interaction background and its interference with the Coulomb interaction on the shape of the $x_\gamma$ distribution;
- the uncertainty associated with the contribution of $\pi\gamma$ events due to the presence of a significant pion component in the separated beam.

Nevertheless, it is assumed that the systematic uncertainty of this first measurement will not exceed in magnitude the statistical one.

## 9. Chiral anomaly study in the $K\gamma \to K\pi$ process

The AMBER experiment with its kaon-enriched beam provides an opportunity to test the predictions of the chiral anomaly in the $K\gamma \to K\pi$ process.

A key distinction from the process involving pions is the two possible configurations of charges: $K^\pm\gamma \to K^\pm\pi^0$ and $K^\pm\gamma \to K^0\pi^\pm$. The chiral anomaly contributes only to the former process and not to the latter, see [66, 67]. A dispersive framework for this process was developed similarly to the $\pi\gamma \to \pi\pi$ process, see [67].

The OKA collaboration in Serpukhov presented the results providing the evidence for the chiral anomaly in kaons [68]. Using a sample of $\sim 8 \times 10^9$ kaons with a momentum of 17.7 GeV/$c$, impinging on a 2-mm-thick copper target, the ratio of the measured $F^{\text{exp}}_{K\gamma K\pi}$ and

the theoretical $F^{th}_{K\gamma K\pi}$ chiral-anomaly constants was obtained by fitting the final state invariant mass distribution for the $K^+\gamma \to K^+\pi^0$ process with the sum of contributions from the chiral anomaly, the $K^*(892)$, and their interference:

$$F^{exp}_{K\gamma K\pi}/F^{th}_{K\gamma K\pi} = 0.9 \pm 0.24_{\text{stat}} \pm 0.3_{\text{syst}}. \tag{19}$$

The main source of the systematics in this result is the impact of the extraction of the number of electromagnetic events by fitting the squared momentum transfer distribution, specifically, the uncertainty in the interference phase between electromagnetic and nuclear coherent events.

Additionally, as mentioned in [67], due to the much higher final state production threshold, the process with kaons has more significant higher-order corrections estimated at 25%.

Assuming the $K^\pm\pi^0$ detection efficiency similar to that of the OKA setup and taking into account the beam energy dependency on the cross section of electromagnetic events, we would expect about $\sim$ 1,000 events for the same beam-integrated flux as the OKA dataset. With the integrated flux of $5 \times 10^{12}$ kaons which is $\sim$ 400 times larger than that of the OKA data taking with the copper target, we expect $\sim 4 \times 10^5$ events of $K\gamma \to K\pi$ to be detected in the AMBER experiment in the range of invariant mass of the final state system below 1.2 GeV/$c^2$. Additional information can be also obtained from analysing the $K^\pm\gamma \to K^0\pi^\pm$ process.

This would allow obtaining the statistical uncertainty on the coupling constant $F_{K\gamma K\pi}$ of $\sim 0.01$ and making a more accurate estimate of the statistical uncertainty arising from the fit of the transferred momentum distributions.

## 10. Summary

The above discussion and the results convincingly confirm a high value of the experimental studies based on the idea to use the Coulomb field of nuclei as a source of quasi-real photons. In the experiments of this type, several important characteristics of hadrons, as well as the interaction between them, have been measured and then compared to the predictions of different theoretical calculations. The particular highlight is that these quantities were introduced and are used for the description of hadron interactions at low energies in the nonperturbative region as an effective low-energy theory of QCD.

Since the early stages of this research, a significant progress has been achieved, and the precision of the theoretical low-energy QCD predictions has been significantly improved. To the very large extent, this was motivated by the increasing precision of the experimental results, in particular, of the above polarizabilities and chiral anomalies measured in different experiments.

It is a pleasure to note that the experimental and theoretical research went hand in hand stimulating each other. And the physicists from JINR have decisively contributed both to theorizing the idea and to implementing it in experiments. The story is still to be continued — we have some more promising proposals to perform measurements with kaons, as well as to improve the precision of the pion quantities already measured.

## Acknowledgements

The authors are grateful to all colleagues who participated in the discussed studies, in particular, the team of the joint JINR–IHEP experiment with the SIGMA spectrometer and the international team of the COMPASS experiment at CERN.

## Conflicts of Interest

The authors declare no conflicts of interest.

## References


[1] M. V. Terent'ev, Electromagnetic properties of pions at low energies, Soviet Physics — Uspekhi 17 (1974) 20–43.

[2] M. V. Terent'ev, Pion polarizability, virtual compton-effect and $\pi \to e\nu\gamma$ decay, Physics of Atomic Nuclei 16 (1972) 162 (in Russian).

[3] M. K. Volkov, V. N. Pervushin, Quantum field theory with a chiral Lagrangian and low-energy meson physics, Physics — Uspekhi 120 (1976) 363 (in Russian).

[4] A. S. Galperin, Yu. L. Kalinovsky, Pion polarizability in the linear sigma-model, JINR Preprint P2-10849, Dubna, 1977 (in Russian).

[5] G. V. Efimov, V. A. Okhlopkova, Pion polarizability in nonlocal quark model, JINR Preprint E4-11568, Dubna, 1978.

[6] A. S. Galperin, G. V. Mitselmakher, A. G. Olshevskiy, V. N. Pervushin, On the possibility of studying pion polarizability in high-energy radiative scattering off nuclei, Physics of Atomic Nuclei 32 (1980) 1053 (in Russian).

[7] H. Primakoff, Photo-Production of Neutral Mesons in Nuclear Electric Fields and the Mean Life of the Neutral Meson, Physical Review 81, 899, Published 1 March, 1951.

[8] Y. M. Antipov, V. A. Bezzubov, N. P. Budanov, Y. P. Gorin, S. P. Denisov, I. V. Kotov, P. A. Kulinich, A. A. Lebedev, G. Mitselmakher and A. G. Olszewski, et al., Observation of the compton effect on $\pi^-$ mesons, Journal of Experimental and Theoretical Physics Letters 35 (1982) 375.

[9] Y. M. Antipov, V. A. Batarin, V. A. Bessubov, N. P. Budanov, Y. P. Gorin, S. P. Denisov, I. V. Kotov, A. A. Lebedev, A. I. Petrukhin and S. A. Polovnikov, et al., Measurement of pi-Meson Polarizability in Pion Compton Effect, Physical Review Letters B 121 (1983) 445–448.

[10] G. A. Akopdjanov, Y. M. Antipov, V. A. Batarin, et al., A setup for investigation of pi meson radiation scattering on nuclei, Preprint IFVE-82-97, Serpukhov, 1982.

[11] Yu. M. Antipov et al., Experimental Evaluation of the Sum of the Electric and Magnetic Polarizabilities of Pions, JINR-P1-84-490, published in Zeitschrift für Physik C26 (1985) 495.

[12] Yu. M. Antipov et al., Study of the Compton effect on the $\pi$-meson and the polarizability of the charged pion, JINR Preprint P1-86-710, 1986.

[13] Yu. M. Antipov et al., Investigation of $\gamma \to 3\pi$ Chiral Anomaly During Pion Pair Production by Pions in the Nuclear Coulomb Field, Physical Review D 36 (1987) 21.

[14] J. Wess, B. Zumino, Consequences of anomalous Ward identities, Physics Letters B 37 (1971) 95–97.

[15] E. Witten, Global Aspects of Current Algebra, Nuclear Physics B 223 (1983) 422–432.

[16] J. Gasser, M. A. Ivanov, and M. E. Sainio, Revisiting $\gamma\gamma \to \pi^+\pi^-$ at low energies, Nuclear Physics B 745 (2006) 84–108.

[17] P. Abbon et al. [COMPASS], The COMPASS experiment at CERN, Nuclear Instruments and Methods in Physics Research Section A 577 (2007) 455–518.

[18] P. Abbon et al. [COMPASS], The COMPASS Setup for Physics with Hadron Beams, Nuclear Instruments and Methods in Physics Research Section A 779 (2015) 69–115.

[19] F. Gautheron et al. [COMPASS], COMPASS-II Proposal, SPSC-P-340.

[20] J. Friedrich, Chiral Dynamics in Pion-Photon Reactions, Habilitation thesis, Munich, Tech. U., 2012.

[21] A. Guskov, Study of meson structure and properties through their interaction with virtual photons in the COMPASS experiment, Habilitation thesis, Dubna, JINR, 2019 (in Russian).

[22] A. V. Guskov, The Primakoff reaction study for pion polarizability measurement at COMPASS, Physics of Particles and Nuclei Letters 7 (2010) 192–200.

[23] C. Adolph et al. [COMPASS], Measurement of the charged-pion polarizability, Physical Review Letters 114 (2015) 062002.

[24] N. Kaiser, Radiative corrections to real and virtual muon Compton scattering revisited, Nuclear Physics A 837 (2010) 87–109.

[25] N. Kaiser and J. M. Friedrich, Radiative corrections to pion-nucleus bremsstrahlung, European Journal of Physics A 39 (2009) 71–80.

[26] N. Kaiser and J. M. Friedrich, Radiative corrections to pion Compton scattering, Nuclear Physics A 812 (2008) 186–200.

[27] N. Kaiser and J. M. Friedrich, Cross-sections for low-energy $\pi^-\gamma$ reactions, European Journal of Physics A 36 (2008) 181–188.

[28] A. B. Arbuzov, Radiative Corrections to High Energy Lepton Bremsstrahlung on Heavy Nuclei, Journal of High Energy Physics 01 (2008) 031.

[29] A. Guskov [COMPASS], Measurement of the charged-pion polarisability at COMPASS, PoS EPS-HEP2015 (2015), 439.

[30] G. Faldt, A Remark on the Primakoff effect, Physical Review C 82 (2010) 037603.

[31] Y. M. Andreev and E. V. Bugaev, Muon bremsstrahlung on heavy atoms, Physical Review D 55 (1997) 1233–1243.

[32] G. Fäldt and U. Tengblad, Coulomb-nuclear interference in pion-nucleus bremsstrahlung, Physical Review C 79 (2009) 014607. [erratum: Physical Review C 87 (2013) No. 2, 029903].

[33] W. Wilcox, Lattice charge overlap. 2: Aspects of charged pion polarizability, Annals of Physics 255 (1997) 60–74.

[34] A. Alexandru, M. Lujan, W. Freeman, F. Lee, Pion electric polarizability from lattice QCD, AIP Conference Proceedings 1701 (2016) No. 1, 040002.

[35] E. V. Luschevskaya, O. E. Solovjeva and O. V. Teryaev, Magnetic polarizability of pion, Physics Letters B 761 (2016) 393–398.

[36] E. V. Luschevskaya, O. E. Solovjeva, O. A. Kochetkov and O. V. Teryaev, Magnetic polarizabilities of light mesons in $SU(3)$ lattice gauge theory, Nuclear Physics B 898 (2015) 627–643; https://doi.org/10.1016/j.nuclphysb.2015.07.023, [arXiv:1411.4284[hep-lat]].

[37] F. X. Lee, A. Alexandru, C. Culver and W. Wilcox, Charged pion electric polarizability from four-point functions in lattice QCD, Physical Review D 108 No. 1, 014512.

[38] L. V. Fil'kov and V. L. Kashevarov, Dipole polarizabilities of charged pions, Physics of Particles and Nuclei 48 (2017) No. 1, 117–123.

[39] L. V. Fil'kov and V. L. Kashevarov, Dipole Polarizabilities of $\pi^{\pm}$-Mesons, International Journal of Modern Physics Conference Series 47 (2018) 1860092.

[40] S. Huber, Upgrade of the COMPASS calorimetric trigger and determination of the charged-pion polarizability, Ph.D. thesis / Munich, Tech. U. (2017).

[41] K. T. Engel, H. H. Patel and M. J. Ramsey-Musolf, Hadronic light-by-light scattering and the pion polarizability, Physical Review D 86 (2012) 037502.

[42] A. Aleksejevs et al., Measuring the charged pion polarizability in the $\gamma\gamma \to \pi^+\pi^-$ reaction. A proposal to the 40th Jefferson Lab Program Advisory Committee, PR-12-13-008 (2013).

[43] V. V. Tarasov, I. F. Larin, CPP/NPP Experiments on Measuring the Polarizabilities of Charged and Neutral Pions., Moscow University Physics Bulletin 79, 580–586 (2024).

[44] B. Pasquini, D. Drechsel and S. Scherer, The Polarizability of the pion: No conflict between dispersion theory and chiral perturbation theory, Physical Review C 77 (2008) 065211.

[45] D. Ecker [COMPASS], Testing predictions of the chiral anomaly in Primakoff reactions at COMPASS, Nuovo Cimento C-Colloquia and Communications in Physics 47 (2024) No. 4, 217.

[46] E. A. Kuraev and Z. K. Silagadze, Once more about the $\omega \to 3\pi$ contact term, Physics of Atomic Nuclei 58 (1995) 1589–1596; [arXiv:hep-ph/9502406[hep-ph]].

[47] M. Hoferichter, B. Kubis and D. Sakkas, Extracting the chiral anomaly from $\gamma\pi \to \pi\pi$, Physical Review D 86 (2012) 116009.

[48] A. Afanasev, J. C. Bernauer, P. Blunden, J. Blümlein, E. W. Cline, J. M. Friedrich, F. Hagelstein, T. Husek, M. Kohl and F. Myhrer, et al., Radiative corrections: from medium to high energy experiments, European Journal of Physics A 60 (2024) No. 4, 91.

[49] Y. M. Antipov, V. A. Batarin, V. A. Bessubov, N. P. Budanov, Y. P. Gorin, S. P. Denisov, S. V. Klimenko, I. V. Kotov, A. A. Lebedev and A. I. Petrukhin, et al., Investigation of $\gamma \to 3\pi$ Chiral Anomaly During Pion Pair Production by Pions in the Nuclear Coulomb Field, Physical Review D 36 (1987) 21.

[50] L. Ametller, M. Knecht and P. Talavera, Electromagnetic corrections to $\gamma\pi^+ \to \pi^0\pi^+$, Physical Review D 64 (2001) 094009.

[51] I. Giller, A. Ocherashvili, T. Ebertshauser, M. A. Moinester and S. Scherer, A New determination of the $\gamma\pi \to \pi\pi$ anomalous amplitude via $\pi^- e^- \to \pi^- e^- \pi^0$ data, European Journal of Physics A 25 (2005) 229–240.

[52] D. V. Amelin et al. [VES], Study of $\eta\pi^-$ production by pions in the Coulomb field, Proceedings of the International Europhysics Conference on High Energy Physics, 1997.

[53] B. Kubis and J. Plenter, Anomalous decay and scattering processes of the $\eta$ meson, European Journal of Physics C 75 (2015) No. 6, 283.

[54] S. Navas et al. [Particle Data Group], Review of particle physics, Physical Review D 110 (2024) No. 3, 030001.

[55] V. N. Pervushin and M. K. Volkov, Pion Polarizability in Chiral Quantum Field Theory, Physics Letters B 55 (1975) 405–408; https://doi.org/10.1016/0370-2693(75)90370-6.

[56] M. K. Volkov and D. Ebert, Pion polarizability in a chiral quark model, Soviet Journal of Nuclear Physics 34 (1981), 104. doi:10.1016/0370-2693(81)90306-3

[57] M. K. Volkov and A. A. Osipov, Polarizability of pions and kaons in superconductor quark model (in Russian), Physics of Atomic Nuclei 41 (1985) 1027–1034.

[58] F. Guerrero and J. Prades, Kaon polarizabilities in chiral perturbation theory, Physics Letters B 405 (1997) 341–346.

[59] S. Nedelko and V. Voronin, Dipole polarizabilities of light pseudoscalar mesons within the domain model of the QCD vacuum, Physical Review D 107 (2023) No. 9, 094027.

[60] M. A. Ivanov and T. Mizutani, Pion and kaon polarizabilities in the quark confinement model, Physical Review D 45 (1992) 1580–1601.

[61] S. Nadeem, W. Wilcox and F. X. Lee, Electric Polarizability of Charged Kaons from Lattice QCD Four-Point Functions, PoS LATTICE2024 (2025) 309.

[62] G. Backenstoss, A. Bamberger, I. Bergström, T. Bunaciu, J. Egger, R. Hagelberg, S. Hultberg, H. Koch, Y. Lynen and H. G. Ritter, et al., $K$- mass and $k$- polarizability from kaonic atoms, Physics Letters B 43 (1973) 431–436.

[63] D. Stamen, J. L. Dammann, Y. Korte and B. Kubis, Polarizabilities from kaon Compton scattering, European Journal of Physics C 84 (2024) No. 12, 1267.

[64] I. Denisenko, A. Guskov and E. Mitrofanov, Hadron structure and spectroscopy at COMPASS. Overview of certain tasks, Physics of Particles and Nuclei 48 (2017) No. 4, 635–658.

[65] B. Adams, C. A. Aidala, R. Akhunzyanov, G. D. Alexeev, M. G. Alexeev, A. Amoroso, V. Andrieux, N. V. Anfimov, V. Anosov and A. Antoshkin, et al., Letter of Intent: A New QCD facility at the M2 beam line of the CERN SPS (COMPASS++/AMBER), 2018.

[66] M. I. Vysotsky and E. V. Zhemchugov, Looking for chiral anomaly in $K\gamma \to K\pi$ reactions, Physical Review D 93 (2016) No. 9, 094029 [erratum: Physical Review D 94 (2016) No. 1, 019901].

[67] D. Stamen, M. Dax and B. Kubis, Dispersive analysis of the Primakoff reaction $\gamma K \to K\pi$, PoS CD2021 (2021), 048.

[68] V. Obraztsov [OKA], Evidence for WZW anomaly in the coherent reaction $K^+Cu \to K^+\pi^0 Cu$ Cu, Journal of Physics: Conference Series 2446 (2023) No. 1, 012047.